Advanced Research and Development Journal
ISSN: **3139-1281**| Volume 2 Issue 1 | January-March 2026 | ARD-004
www.ardjournal.com | DOI: https://doi.org/10.5281/zenodo.22304491

BAND-TO-BAND TRANSITIONS AND CRITICAL POINTS IN THENEAR-INFRARED TO VACUUM ULTRAVIOLET DIELECTRIC FUNCTIONS OF SINGLE CRYSTAL URANIA AND THORIA

B.SAIRAM, *IoT Engineer,*
NEWZEN INFOTECH, HYDERABAD

ABSTRACT: Critical-point dielectric function investigations and spectral ellipsometry were utilized to compare and find the band-to-band transition energy values for single-crystal actinide samples of thorium oxide and uranium oxide. We used spectroscopic ellipsometry to investigate the dielectric characteristics of thorium oxide and uranium oxide over a wide range of wavelengths, from deep ultraviolet to near-infrared. UO2 has a critical point structure comparable to ThO2, however ThO2's is much more blue-shifted. ThO2 has a bandgap energy of 5.4 eV, while UO2 has a bandgap energy of 2.1 eV.
Keywords: Band, Vacuum, Ultraviolet, Dielectric , Urania, Thoria

1.INTRODUCTION

Uranium dioxide (UO2) and thorium dioxide (ThO2) have recently received renewed consideration as possible semiconductors for neutron detectors.1, 2 The optical and electrical characteristics of ThO2 are yet unknown. Furthermore, understanding of UO2 is limited. Until recently, experimental study on the optical and electrical properties of UO2 and ThO2 was limited due to a shortage of high-quality single-crystal samples. We identified these structures in our previous investigation by comparing the high-quality ordered structures of nearly stoichiometric UO2 discovered in previous research on these materials using methods such as core level photoemission spectroscopy and others to those of growth by alternative processes.8 This study expands on previous research by utilizing near-stoichiometric UO 3,5,9,10 and ThO 6,7,9, allowing for a thorough exploration of their optical characteristics.

There has been little investigation into the optical characteristics of UO2 spanning the near-infrared to ultraviolet spectrum. Schoenes measured the reflectance of single crystals of UO2 to be between 0.03 and 13 eV. NUMBER 14 e1 ie2 was the complex-valued dielectric function she calculated using numerical Kramers-Kronig integrals.8 Meek et al. examined the transmission and absorption properties of UO2 films.He et al. used spectroscopic ellipsometry and density functional theory to explore the bandgap of uranium oxide thin films of various compositions.12 Specroscopic ellipsometry was used by Dugan et al.3 and Siekhaus and Crowhurst13 to determine the critical-point structures in e. Critical-point formations are caused by electronic band-to-band transitions and are linked to singularities in the aggregate density of states.14 Critical-point features include widening, amplitude, and critical-point transition energy. Singularities take several forms depending on the type of band structure. Previous research on UO2 has revealed significant changes in optical critical-point properties as evaluated by ellipsometry and reflexivity (8.3, 13). No optical property measurements of ThO2 have been reported as of yet. Thorium and uranium have similar

Advanced Research and Development Journal
ISSN: **3139-1281**| Volume 2 Issue 1 | January-March 2026 | ARD-004
www.ardjournal.com | DOI: https://doi.org/10.5281/zenodo.22304491

valence electron configurations, with thorium having four electron configurations and uranium having six ([Rn] 5f3 6d1 7s2). Their oxides have a cubic (feldspar-like) structure and homogeneous unit cell sizes. Through spectroscopic ellipsometry examinations covering the near-infrared to vacuum ultraviolet spectral range, researchers can now compare the dielectric properties of single-crystal ThO2 and UO2. The band-to-band transition parameters obtained from the examination of the two actinide oxides were investigated. The dielectric functions were also subjected to a critical-point study.

Data processing must include the application of appropriate physical models in order to extract critical physical information from spectroscopic ellipsometric data.15 Mode of polarization Due to their optical isotropy, conversion from parallel (p) to perpendicular (s) does not occur during light reflection from the surfaces of single crystals UO2 and ThO2. Single-crystal actinides were regarded to be optically thick, quasi-half-finite substrates, hence the approximation of the substrate-ambient boundary condition was used.16 The finite irregularity at the single crystal-ambient interface, which influences spectroscopic ellipsometry measurements, must be taken into account. Mechanically polished single crystal surfaces, in particular, have long-lasting surface fault zones. An effective over-layer with effective thicknesses significantly less than the wavelengths and effective dielectric function values was able to recreate the effects of physical surface irregularity by using an effective medium approximation.16 Surface roughness layer thickness and average physical roughness surface height variation commonly coincide.17 By altering the volume ratio, the average value of e (single crystal actinide with vacancy, designated as e 1) was calculated in order to determine the dielectric function of the surface roughness layer. As model parameters, the thickness of the surface roughness layer and the real and imaginary components of e for each wavelength are to be computed. Every unknown parameter was discovered using a wavelength-by-wavelength regression analysis.

The optical critical-point characteristics determine the spectral structure of the dielectric function of materials in the band-to-band transition spectral region. Model dielectric function techniques can be used to illustrate structural critical spots. Five Gaussian-broadened oscillators indicate the critical-point features; n represents the imaginary component of their individual critical-point contributions.

$$\varepsilon_2(E) = \sum_{n=1}^{N} \mathrm{A}_n \left[e^{-\left(\frac{E-\mathrm{E}_n}{\sigma_n}\right)^2} - e^{-\left(\frac{E+\mathrm{E}_n}{\sigma_n}\right)^2} \right], \qquad (1)$$

Located in

$$\sigma_n = \frac{\mathrm{B}_n}{2\sqrt{ln(2)}}, \qquad (2)$$

The Kramers-Kronig integration produces the actual component of e.

$$\varepsilon_1(E) = \varepsilon_\infty + \frac{2}{\pi} P \int_0^\infty \frac{\xi \varepsilon_2(\xi)}{\xi^2 - E^2} d\xi. \qquad (3)$$

The symbols An, En, and Bn represent the nth-critical-point amplitude, transition energy, and transition broadening parameters, respectively. E1 indicates the dielectric function's static

Advanced Research and Development Journal
ISSN: **3139-1281**| Volume 2 Issue 1 | January-March 2026 | ARD-004
www.ardjournal.com | DOI: https://doi.org/10.5281/zenodo.22304491

contribution, whereas E.3,18 represents photon energy.

For the purposes of this study, single crystals of ThO2 and UO2 were synthesized via hydrothermal synthesis. ThO2 and UO2 growth methods were very comparable in terms of mineralizer solution, pressure, and temperature. The mineralizer in both growth procedures was a 6M cesium fluoride solution (Alfa Aesar, 99.99%). Sealing Systems Inc. supplied growth processes with sealed silver ampoules (99.95% Ag) to limit the possibility of contaminants penetrating the Inconel autoclave walls. Both ends were securely welded and sealed. A silver seed rack was used to hang a ThO2 seed crystal in the upper portion of the silver tube in order to get the ThO2 sample. The lower portion of the tube, separated from the seed crystal by a porous silver barrier, contained a charge of ThO2 nutrient/feedstock (99.99% thorium oxide, International Bio-analytical Laboratories). By preventing heat mingling, the barrier keeps two distinct temperature zones within the tube. The silver tubes were then placed in a 250 ml Inconel autoclave. To prevent the mineralizer solution's pressure from rupturing the silver tube, 80 to 85 percent of the remaining capacity was supplied with counter-pressure water.The autoclave was outfitted with two temperature zones, one for the feedstock and one for the seed crystals, thanks to the use of band heaters. The cesium iodide solution dissolves the feedstock at higher temperatures (dissolution) to produce a saturated solution. As the temperature of the seed crystal (crystallization zone) was reduced, a spontaneous convection flow was formed, facilitating the transport of the saturated solution towards the chilly region. ThO2 forms on the seed crystal as a result of the supersaturated solution precipitating at the lower temperature. The dissolution zone temperature for ThO2 was 650 C, while the crystallization zone temperature was kept at 600 C, resulting in a pressure of 172 MPa. It lasted for a period of ninety days. The ThO2 seed crystal was taken from the silver tube when it had chilled, and any calcium fluoride mineralizer that remained was washed away. In the absence of significant UO2 seeds or substrates, the UO2 sample was also grown on a ThO2 seed crystal. Throughout the 50-day growth period employing the UO2 (99.998% uranium oxide, International Bio-analytical Laboratories) growth procedure, the mineralizer solution, temperatures, and pressures were constant.

Both specimens were polished before being lowered to the (100) crystallographic plane. The specimens were sonicated with deionized water and acetone to remove any remaining crystal bonds and loose particles.

The lattice characteristics of ThO2 and UO2 were determined by single crystal X-ray diffraction (XtaLAB mini, Rigaku). Due to the large size of the ThO2 and UO2 crystals utilized in the ellipsometry studies, direct calculation of lattice parameters was not possible. The characteristic lattice properties of ThO2 and UO2 were measured after they were spontaneously formed into smaller crystals under comparable growth conditions. The lattice parameter of ThO2 was 5.6070 6 0.0006 A, which corresponded to the predicted value of 559.7 pm.19 Prior study identified UO2's lattice parameters as (5.4703 6 0.0006) A, which corresponds to the stoichiometry UO2.003.20,21. The supplementary materials include further data and discussion that supports the stoichiometric character of the aforementioned samples.

Spectroscopic ellipsometry data were collected from 0.75 eV to 6.4 eV using a dual-rotating

Advanced Research and Development Journal
ISSN: **3139-1281**| Volume 2 Issue 1 | January-March 2026 | ARD-004
www.ardjournal.com | DOI: https://doi.org/10.5281/zenodo.22304491

compensator ellipsometer (RC2, J. A. Woollam Co., Inc.), as shown in Figures 1 and 2. Seven angles of incidence (Ua 45, 50, 55, 60, 65, 70, and 75) were used to collect data; however, only three are shown for clarity because they are all incorporated into the data analysis. This instrument's spectral resolution is one nanometer.

Data were collected in the spectrum area spanning 5 eV to 9 eV using a nitrogen-purged rotating analyzer ellipsometer (VUV-VASE, J. A. Woollam Co., Inc.). Data were collected at three incidence angles (Ua 50, 60, and 70) at this location. This measurement's resolution has been set at 0.02 eV. Furthermore, despite the large overlap in the acquired data range, we only show data from 6.5 eV and above in Figures 1 and 2, with a dashed vertical line indicating the changeover.

Figures 1 and 2 show experimental (symbols) and best-match model derived (solid lines) spectroscopic ellipsometry data for solitary crystals of UO2 and ThO2, respectively. The data are for various incidence angles. There is excellent agreement between experimental data and model simulation data. Model simulation results were achieved by measuring effective layer thickness and surface roughness wavelength by wavelength. Under the assumption that the UO2 crystal is generated from a volumetric mixture of void and UO2 material in a 50:50 ratio (dielectric function), the roughness effective layer thickness is calculated to be roughly 4 nm. We find a roughness effective layer with a vacuum-to-ThO2 volume ratio of 10:90 and effective roughness layer thickness values of approximately 10 nm and 20 nm, which differ from the VUV and RC2 approaches.

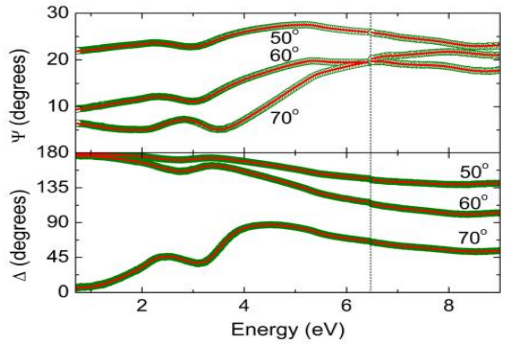

FIG. 1. Experimental (open symbols: Ψ, closed symbols: Δ) and best-match model calculated spectroscopic ellipsometry data (solid lines) for spectroscopic ellipsometry data measured at multiple angles of incidence for the UO_2 single crystal sample. The dashed vertical line indicates instrument switch at 6.5 eV.

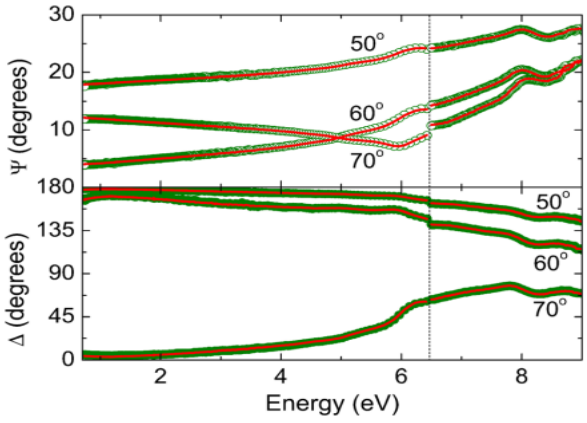

FIG. 2. Same as Fig. 1 for the ThO_2 single-crystal sample.

Advanced Research and Development Journal
ISSN: **3139-1281**| Volume 2 Issue 1 | January-March 2026 | ARD-004
www.ardjournal.com | DOI: https://doi.org/10.5281/zenodo.22304491

These variations are caused by surface effects induced during crystal refining operations. To account for the submicroscopic surface imperfection that leads to the angular dispersion of the reflected measurement beams, the apertures of the two instruments are added into the model analysis. This change to the model analysis compensates for a reflected beam with a dispersion that spans the entire angle of incidence, which is equivalent to the detector's entrance aperture. The near-IR-VIS instrument, on the other hand, has a smaller entrance (about 3) than the VUV instrument (caliber 8). As a result, a tiny offset in the ellipsometry data between the two instruments is noticed for the ThO2 sample (see Figure 2). Because this offset is purely instrumental and originates from surface irregularity, both effects are quantitatively eliminated, as seen in Figure 4's dielectric function for ThO2. Figures 3 and 4 show the actual

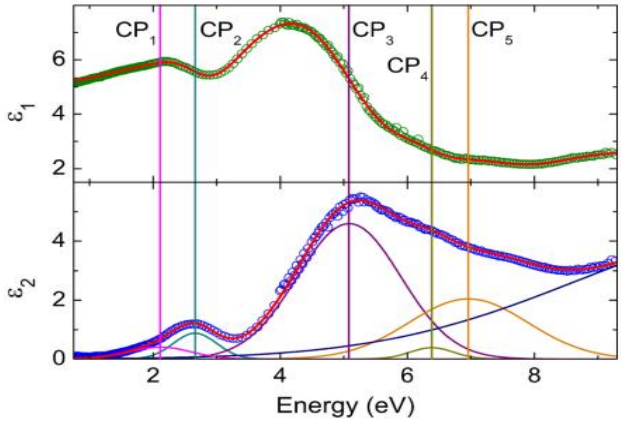

FIG. 3. Real (green symbols) and imaginary parts (blue symbols) of ε for the UO_2 single-crystal sample obtained from the wavelength-by-wavelength spectroscopic ellipsometry data analysis. Shown in comparison are the individual (solid lines) and total (red lines) critical-point transition contributions. Vertical lines indicate the individual critical-point transition energy parameters.

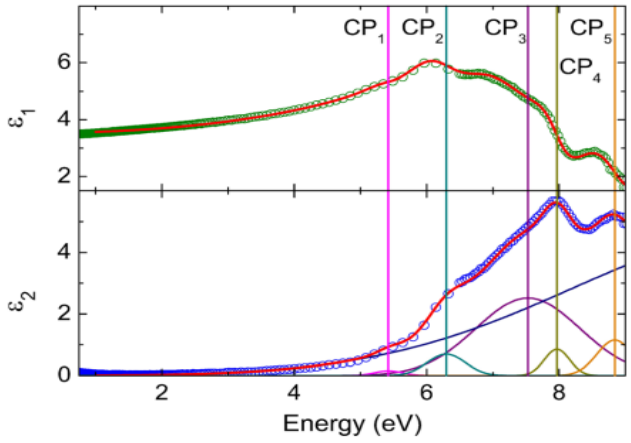

FIG. 4. Same as Fig. 3 for the ThO_2 single-crystal sample.

This we obtained by analyzing ThO2 and UO2 data, as well as the potential components of e denoted by the symbols. In both samples, an imaginary component of the dielectric response disappears in the near-infrared spectrum. This shows that a semiconductor material with a persistent bandgap energy is present. In the dielectric function of ThO2, right below the bandgap, a protracted tail-like structure may be seen. This implies that the ThO2 sample may have crystalline flaws.

The predicted critical-point contributions from the best-match model, which were determined during the critical-point model analysis, are likewise shown as solid lines in Figures 3 and 4.

Advanced Research and Development Journal
ISSN: **3139-1281**| Volume 2 Issue 1 | January-March 2026 | ARD-004
www.ardjournal.com | DOI: https://doi.org/10.5281/zenodo.22304491

In Figures 3 and 4, color-coded vertical lines in the imaginary portion of the dielectric functions depict the critical point contributions and accompanying energy parameters from the band to the transition center. Each Gaussian oscillator's center energy, denoted as En, can be calculated. Furthermore, a faithful approximation of the functions e calculated wavelength-by-wavelength for UO2 and ThO2 may be produced. Tables I and II contain a complete list of critical-point parameter values for the single-crystal examples of ThO2 and UO2 studied over the whole wavelength range. The imaginary region of the ThO2 dielectric function located below the bandgap has a noticeable tail. The tail has an extremely broad-ranging Gaussian oscillator that is centered at energy levels beyond the wavelength range under study. It has every change at higher energy that effects the dielectric function, as well as another oscillator that works in the same way.

TABLE I. Critical-point parameters: amplitude (A_n), transition energy (E_n), and broadening (B_n) for the UO_2 dielectric function within the investigated spectral region. Digits in parentheses indicate the 90% confidence interval obtained from numerical best-match model analysis. A static contribution to the dielectric function near unity 1.02 ± 0.02 was found for the real part of the dielectric function of UO_2.

n	A_n (eV)	E_n (eV)	B_n (eV)
1	0.4 (0)	2. (1)	1. (1)
2	0. (8)	2.6 (6)	0.8 (0)
3	4.5 (9)	5.0 (8)	1.9 (3)
4	0.3 (9)	6.3 (9)	0.8 (1)
5	2.0 (4)	6.9 (6)	2.2 (1)

TABLE II. Same as Table I for ThO_2. A static contribution to the dielectric function of 1.01 ± 0.01 was determined for the real part of the dielectric function of ThO_2.

n	A_n (eV)	E_n (eV)	B_n (eV)
1	0.1 (2)	5.4 (4)	0.4 (3)
2	0.6 (7)	6.3 (5)	0.6 (6)
3	2.2 (3)	7.5 (0)	1.6 (3)
4	1.1 (8)	7.96 (5)	0.4 (5)
5	0.9 (9)	8.82 (6)	0.5 (9)

In addition, in the UO2 critical point analysis, an energy-rich center was used.

Both actinide oxides exhibit five distinct critical-point properties when inspected optically. The integers n 1, 2, 3, 4, and 5 represent these, with the values increasing with the transition energy. In Figures 3 and 4, these qualities are denoted by the same color designations. In all instances, the third-most important changes in the functioning of each dielectric function occur at the crucial points (n 3). As previously noted, ThO2 and UO2 share numerous characteristics; this work adds to that evidence. This statement holds true despite modest differences in valence electron configurations between thorium and uranium [Rn] 5f 3 6d1 7s2 and [Rn] 6d2 7s2. Because of the unexpected non-bonding of their 5f electrons, both

Advanced Research and Development Journal
ISSN: **3139-1281**| Volume 2 Issue 1 | January-March 2026 | ARD-004
www.ardjournal.com | DOI: https://doi.org/10.5281/zenodo.22304491

ThO2 and uranium have a cubic crystalline structure; nevertheless, ThO2 has a marginally higher lattice constant.The critical point transition energy for EThO2;1 is 5:4 eV, while EUO2;1 has the lowest at 2:1 eV. The energies at issue are the bandgap energies, which are the basic band-to-band transition energy of all oxides. Despite its many similarities, the substance with the greater bandgap (ThO2) clearly has more noticeable and closely spaced critical points. As one would expect from a big bandgap oxide. The previously reported band structure simulations predicted a bandgap energy of 2.19 eV for UO2, which is in great agreement with the critical-point transition energy measured by measurements.The band structure of ThO2.22-24 has received much attention. The computed bandgap values cover a wide energy range, ranging from 3.3 to 6.9 eV. The experimental measurement of 5.4 eV appears to differ from a previously reported figure. In contrast, it appears to be located in the middle of this broad spectrum. As a result, exceptional single-crystal actinide oxide samples of thorium oxide and uranium oxide were made and studied for their light absorption properties. The dielectric characteristics of both oxides were evaluated using spectroscopic ellipsometry. These functions apply to critical-point formations that have similar appearances but differ in photon energy. Each of the molecules is affected by five important parameters. ThO2 and UO2 have the lowest bandgap energies, measuring 5.4 eV and 2.1 eV, respectively. Every time ThO switches from one band to the next, UO experiences a 2 to 3 eV blue shift.Consult the supplemental materials for more information on the stoichiometry, electrical structure, and sample quality of thoria and urania.

This study was funded in part by the Nebraska Materials Research Science and Engineering Center (Award No. DMR 1420645) and the National Science Foundation (Award No. DMR 1808715). The Defense Threat Reduction Agency of the Air Force (Grant No. HDTRA1-14-1-0041) and the Department of Homeland Security's Domestic Nuclear Detection Office (Grant No. HSHQDC14X00089) separately donated funds to this initiative. The US Department of Energy's Office of Science and Office of Basic Energy Sciences provided funding for the Center for Thermal Energy Transport under Irradiation. An Energy Frontier Research Center assisted J.M.M. The J. A. Woollam Foundation helped in many ways, and A.M., S.K., R.K., and M.S. are grateful. The XPS photoemission data in the supplemental material were obtained with the help of Daniel Felker, Eric Hunt, J. W. McClory, T. D. Kelly, D. Turner, J. W. Kolis, and Xin Zhang. This is something the authors are grateful for. This article contains the authors' ideas and views, which may not necessarily reflect those of the US Air Force, the Department of Defense, or the US government.

REFERENCES

1. T. T. Meek and B. von Roedern, Vacuum 83, 226 (2008).
2. C. Kruschwitz, S. Mukhopadhyay, D. Schwellenbach, T. Meek, B. Shaver, T. Cunningham, and J. Auxier, Proc. SPIE 9213, 92130C (2014).
3. C. L. Dugan, G. G. Peterson, A. Mock, C. Young, J. M. Mann, M. Nastasi, M. Schubert, L. Wang, W.-N. Mei, I. Tanabe, P. A. Dowben, and J. Petrosky, Eur. Phys. J. B 91, 67 (2018).
4. M. Mann, D. Thompson, K. Serivalsatit, T. M. Tritt, J. Ballato, and J. Kolis, C. Young, J. Petrosky, J. M. Mann, E. M. Hunt, D. Turner, and P. A. Dowben, J. A. Colon Santana,

Advanced Research and Development Journal
ISSN: **3139-1281**| Volume 2 Issue 1 | January-March 2026 | ARD-004
www.ardjournal.com | DOI: https://doi.org/10.5281/zenodo.22304491

and P. A. Dowben, in MRS Symposium Proceedings, 2013, Vol. 1576.

5. T. Kelly, J. Petrosky, D. Turner, J. McClory, J. Mann, J. Kolis, X. Zhang, and P. D. Turner, T. Kelly, G. Peterson, J. Reding, R. Hengehold, J. Mann, J. Kolis, X. Zhang, P. Dowben, and J. Petrosky, Phys. Status Solidi B 253, 1970 (2016).
6. K. K. Gajula, "Quantum-Enhanced Cryptographic Protocols for Ultra-Secure Data Transmission in Next-Generation Networks," Journal of Dalian University of Technology, vol. 31, no. 12, 2024.
7. C. Young, J. Petrosky, J. M. Mann, E. M. Hunt, D. Turner, and T. Kelly, Phys. T. Meek, B. Von Roedern, P. Clem, and R. Hanrahan, Jr., Mater. Lett. 59, 1085 (2005).
8. H. He, D. A. Andersson, D. D. Allred, and K. D. Rector, J. Phys. Chem. C 117, 16540 (2013).
9. W. Siekhaus and J. Crowhurst, in IOP Conference Series: Materials Science and Engineering (IOP Publishing, 2010), Vol. 9, p. 012055.
10. P. Yu and M. Cardona, Fundamentals of Semiconductors (Springer, Berlin, Heidelberg, New York, 2005).
11. H. Fujiwara, Spectroscopic Ellipsometry (John Wiley & Sons, New York, 2007).
12. M. K. Srinivasan and K. K. Gajula, "Comprehensive and Empirical Evaluation of Classical Annealing and Simulated Quantum Annealing in Approximation of Global Optima for Discrete Optimization Problems," ICT with Intelligent Applications: Proceedings of ICTIS 2021, vol. 1, pp. 165–181, 2021.
13. K. K. Gajula, "Advancing Post-Quantum Cryptography: Novel Algorithmic Models and Security Implementations," Goya Journal, vol. 18, no. 12, pp. 594–605, 2025.